water

Article

A Conceptual Model to Quantify the Water Balance Components of a Watershed in a Continuous Permafrost Region

Alain Lubini Tshumuka * and **Musandji Fuamba**

Department of Civil, Geological and Mining Engineering, Polytechnique Montréal, Montréal, QC H3T 1J4, Canada; musandji.fuamba@polymtl.ca
* Correspondence: alain.lubini-tshumuka@polymtl.ca

Abstract: In regions characterized by continuous permafrost, hydrological modeling remains a complex activity, primarily due to constraints related to the prevailing climatic conditions and the specific behavior of the active layer. High-latitude regions receive less solar radiation; thus, most creeks are active only during summertime and stay frozen in the winter. To realistically simulate watersheds underlain by continuous permafrost, the heat transfer through the soil needs to be accounted for in the modeling process. In this study, a watershed located in a continuous permafrost zone in Russia is investigated. A model is proposed to integrate this heat transfer into an existing conceptual rain-flow transformation model, Hydrologiska Byråns Vattenbalansavdelning (HBV), to calculate the seasonal thaw depth and determine the components of water balance. The proposed integration is a novelty compared to the standard model, as it enables the physical and thermal properties of the soil to be taken into account. It was found that the proposed model, HBV-Heat, performs better than the stand-alone HBV model. Specifically, the average Nash–Sutcliffe efficiency (NSE) increases by 30% for the whole calibration period. In terms of the water balance components, the results are consistent with previous studies, showing that surface runoff represents 64% of the observed precipitation.

Keywords: continuous permafrost; heat transfer; hydrological modeling; thaw depth; water balance

check for updates

Citation: Lubini Tshumuka, A.; Fuamba, M. A Conceptual Model to Quantify the Water Balance Components of a Watershed in a Continuous Permafrost Region. *Water* **2024**, *16*, 83. https://doi.org/10.3390/w16010083

Academic Editor: Achim A. Beylich

Received: 20 November 2023
Revised: 21 December 2023
Accepted: 21 December 2023
Published: 25 December 2023

1. Introduction

Catchments located in areas of continuous permafrost are characterized by a thermal state that keeps the ground frozen for at least two consecutive years. This characteristic greatly reduces the hydrological activity of these areas for a long time period [1]. In these areas, when conditions allow, groundwater flows mainly through the active layer, i.e., the part of the ground between the surface and the ice cover, which undergoes a seasonal freeze–thaw cycle. An analysis of the hydrological response of such a basin requires that this important aspect of soil dynamics be considered and integrated into a groundwater or surface flow model [2]. This integration is essential because the infiltration process, on which flow generation depends, is highly influenced by the status of the ground. In general, the state of the ground is defined by the thermal state of the soil, its hydro-physical properties, temperature, the initial moisture content, and the amount and rate of release of water from melting snow [3,4] From the above factors, the water content is directly related to the depth of thaw, whose extent determines the soil's storage capacity. Given the undeniable influence of the thermal regime on soil water storage and movement, several studies have demonstrated the value of incorporating the heat transfer equation into hydrological modeling. In this regard, [5] noted that an explicit consideration of the thermal regime of the ground presents a particular challenge to permafrost hydrological modeling.

Addressing this challenge by integrating the active layer's freeze–thaw process into a physically-based hydrological model involves solving the heat transfer equation in a porous medium with moving boundary conditions. Due to its simplicity, the original Stefan's analytical solution [6,7] and subsequent modifications [8–15] have been incorporated into several models. Although the computational time is short, this modeling approach has limitations that are inherent in the assumptions underlying the derivation of this analytical solution [16]. In addition, models derived from this approach do not account for soil stratification, heat capacity, or other factors that affect the rate of soil freezing and thawing [17].

Faced with this limitation, the approach of integrating a numerical solution with a physical or conceptual hydrological model presents itself as an alternative. This kind of solution considers the heterogeneity of soil layers to account for phase changes. It is also able to handle the mixing zone containing the liquid–solid mixture and is more accurate than analytical models [18]. Elaborated examples of numerical solutions derived from this approach can be found in [19–21]. However, the integration of numerical solutions into a surface-water flow model increases the computational time. This latter aspect remains a challenge for any study aimed at modeling northern basins. In this context, the present study proposes to couple a thaw depth determination algorithm presented in a previous study [22] with the Hydrologiska Byråns Vattenbalansavdelning (HBV) conceptual model [23]. The HBV model is chosen for its versatility in terms of the diversity of the geographical areas in which it has been applied [21], its simplicity in terms of the modules describing different hydrological processes [24,25], and its relatively limited application in permafrost environments. In this regard, Ref. [23] pointed out that applications of the HBV model have led to an intuitive conclusion that the effect of frozen ground is either considered in the analysis of existing free parameters or that it is of minor importance for performance. The main objective of the present study is to model the hydrological response of a basin in a continuous permafrost zone using an approach characterized by the integration of a heat transfer module into an existing conceptual model. Obviously, the novelty of this study lies in this aspect, as the proposed approach takes the physical and thermal properties of the soil into account. This methodology significantly enhances the capabilities of the existing tool and expands its scope.

Ref. [11] suggested that an accurate simulation of the timing and depth of the freeze–thaw boundary in land surface models will improve their ability to model not only soil temperature, soil moisture, and runoff/infiltration hydrology, but also energy, water, and greenhouse gas exchange processes in high latitudes.

The current study's relevance stems from its ability to comprehend the elements of a basin's water balance in a continuous permafrost region. As a result, the results of hydrological modeling can be used to evaluate water availability, assess potential climate change effects on water resources, and develop effective water management strategies.

In line with the main objective, the present study focuses on the following aspects, among other things:

- Simulation of seasonal thaw depths;
- Comparison between the existing model and the proposed model;
- Establishment of the water balance components of the catchment.

2. Materials and Methods

2.1. Study Area

In the present study, the water balance components of a catchment in the Kolyma station in Siberia, Northeast Russia, are determined. The main watercourse is the Kontaktovy Creek, which rises in the Morozova Mountains at an altitude of over 1400 m and flows into its outlet at an altitude of 823 m. The catchment area under study is the eastern part of the watercourse (Figure 1). The area of the catchment delimited by the gauging station (61 N, 147 E) is 14.2 km^2, while the basin as a whole has an area of 21 km^2. The study site is a watershed located in the area of continuous permafrost and has been described in Refs. [26–28]. The corresponding permafrost data, such as freeze–thaw depth measurements, soil temperature at different depths, and standard hydrometeorological data, were collected from 1948 to 1997. The climate in the area is continental, with long winters, warm summers, and precipitation that falls mainly as snow. The average temperature at the Nizhnyaya meteorological station is −11.4 °C, with an average of 130 days with temperatures above freezing. The mean annual precipitation is 314 mm [29]. The site is mountainous, located in the transitional zone between the forest-tundra and coniferous taigas on very diverse soil, which mainly varies from rock debris to clay podzol with partially decomposed organic material underlain by frozen soil and bedrock [30].

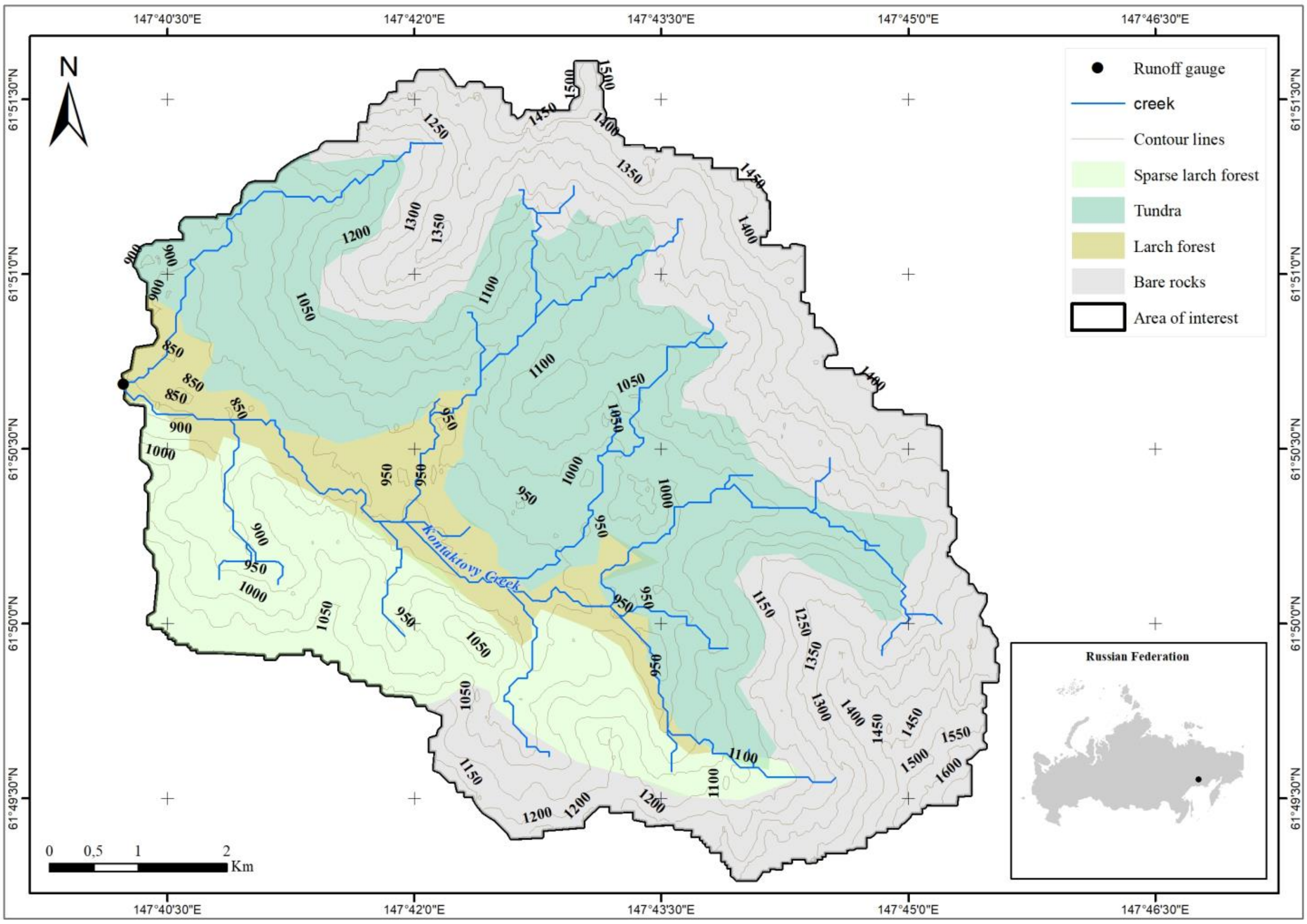

Figure 1. Study area—Kontaktovy Creek watershed.

2.2. Description of the HBV Model

The HBV model is a simple conceptual rainfall-runoff transformation model developed by Bergström and Forsman [31]. The model has a simple structure and comprises a snow accumulation and ablation routine, soil moisture accounting, runoff generation, and a hydrograph transformation routine. The model parameters are either physically or empirically based.

Typically, daily precipitation in the form of rain and snow with monthly long-term estimates of the potential evaporation rate is used as input to the model.

The snow module uses the temperature-index approach to estimate snowmelt as a linear function of air temperature. Then, meltwater and rainfall are fed into the soil moisture routine to simulate groundwater recharge and actual evaporation as functions of actual water storage. The runoff generation is simulated by the response routine as a function of water storage. The whole modeling process culminates in the routing routine, where runoff to the catchment outlet is simulated using a triangular weighting function.

To date, several versions of this model have been presented. Ref. [28] reports that, in addition to the original model produced by the Swedish Meteorological and Hydrological

Institute (SMHI), seven different versions have been used in recent scientific publications. This model has been used in various catchments for all kinds of hydrological analyses, including flood forecasting, hydroelectric dam projects, and climate change studies [32–34]. It should be noted that while the model has been used in many Nordic basins, very few studies, a total of eight in the last decade, have been carried out in the Arctic regions [35].

The HBV model can operate as a global model (with a single basin) or as a distributed/semi-distributed model, and in the latter case, differentiation appears not only in the elevation but also in the characterization of the sub-basins. More details on the description of the model are available in [20,36].

2.3. Data Collection and Processing

The HBV model requires meteorological data (precipitation, temperature, and evapotranspiration) to simulate the basin's hydrological response (the discharge) at the outlet. In this section, information about the source of data is provided, and their important characteristics are highlighted.

2.3.1. Meteorological Data

The meteorological data used for the simulations were taken from the Nizhnyana station, located at coordinates (60 N, 147 E), and are available from the Pangaea Data Publisher for Earth & Environmental Science, Ref. [37]. The daily input precipitation and temperature data cover an 11-year period, from 1960 to 1965 (calibration period) and from 1977 to 1981 (validation period). The data were subjected to quality control, but no corrections were made. No inconsistencies were found, and there were no missing values; therefore, these data were used for the entire watershed.

An analysis of the temperature data for the period of 1960–1965 shows that the annual minimum values vary between −50.1 °C and −44.2 °C, while the observed annual maximum temperature varies between 17.5 °C and 19.6 °C. Since the HBV model uses precipitation in solid or liquid form, temperature is used to determine the type of precipitation, for which a threshold temperature must first be determined. The period of negative air temperature lasts from October to April, and the freeze-free period is 130 days on average [30]. The total annual precipitation varies from 277.14 mm to 369.65 mm, while the maximum annual rainfall varies between 15.1 mm and 32.89 mm.

2.3.2. Runoff

It must be noted that, as the catchment lies in a continuous permafrost zone, there is no flow in winter due to ice and snow in the riverbed. The daily data are taken from the Kolyma gauging station (KWBS_runoff_1102, latitude of 61.84000 N and longitude of 147.67000 E) and are available for the period between the end of May and the end of September. The hydrological season is very short, with a peak discharge observed at the beginning of the warm season, just after snowmelt and other peaks caused by rainfall have occurred.

During the period 1960–1965, the maximum measured peak discharge was 2.54 m^3/s, while the lowest annual peak and average daily discharge of the series were 1.43 m^3/s and 0.24 m^3/s, respectively. In general, after the winter freeze-up period, the river flows again in the second half of May. However, there is a time lag between the onset of snowmelt and the moment when significant flow is observed in the watercourse. The presence of depressions, soil conditions, and distance from mountainous areas could explain this time lag.

An analysis of the flows observed over the period 1977–1981 shows that the maximum flow reached was 4.57 m^3/s, while the minimum value for this period was 2.21 m^3/s. A comparison between the calibration and validation periods shows a 55% increase in the lowest annual maximum discharge. This increase is even more pronounced, at 80%, when comparing the maximum annual flow of the two periods. This clear difference can be explained by the corrections made to the observed values from 1968 onward; no corrections were made to the data prior to that year.

2.4. Heat Transfer Model

2.4.1. Heat Transfer Model Description

The heat transfer module used for modeling phase-change porous media was developed and presented in [22]. In this model, only conduction is used as the heat transfer mode. The calculations assume that the soil is initially frozen and then thaws suddenly when the temperature is above the freezing point. This is a phase change problem that involves a moving boundary condition. The aim of solving this problem is to determine the temperature distribution in the soil and the location of the interface between the two phases (solid and liquid). This problem, also known as Stefan's problem, is non-linear by nature and has very few exact solutions. Given the difficulties encountered in solving it, an alternative approach is to reformulate the problem and present it in the form of an enthalpy equation, as follows:

$$\frac{\mathrm{dH_i}}{\mathrm{dt}} = \nabla\cdot(\lambda_\mathrm{i}\nabla \mathrm{T_i}) + \theta \tag{1}$$

where $d(\cdot)/dt$ represents the Lagrangian derivative, ∇ is the nabla operator, and H_i; λ_i, and T_i denote the total enthalpy (J), thermal conductivity (W/m.k), and temperature (°C) for every single phase i, respectively.

The total enthalpy is a function of the temperature and can be expressed in one equation that regroups all phases as a sum of sensible heat and latent heat.

$$H\ (T) = \int_{T_r}^{T} < C > dT + \rho_l \phi L_f \tag{2}$$

L_f represents the latent heat of fusion (J/kg), while ρ_l is the density of the liquid (kg/m^3); C and ϕ are the volumetric heat capacity (J/(m^3·K) and the volumetric local liquid fraction, respectively. The derivative of Equation (2) leads to the following relation, which serves as the basis for the numerical approximation:

$$\tilde{C}\frac{dT}{dt} = \nabla\cdot(< \lambda > \nabla T) + < S_T > \tag{3}$$

where $\tilde{C}$ is given by $\left(< C > + \rho_l L_f \frac{d\phi}{dT}\right)$.

Equation (3) and the boundary conditions were solved numerically using an implicit finite difference discretization.

The module is based on an enthalpy-porosity model whose governing equations and boundary conditions are discretized using the finite difference method. During the iterative process leading to the results, an artificially mixed zone consisting of the solid and liquid phases is maintained with the same thickness by keeping the regularization parameter proportional to the temperature gradient. In this study, the obtained implicit model was validated by comparing the simulation results, firstly, with Stefan's analytical solution and, secondly, with the results of a model obtained using an explicit scheme.

The validation was completed by applying the model in the field (Kolyma water-balance station, Russia) using four different soil profiles. Each of the soil profiles consisted of layers of different compositions, allowing the model to be evaluated in homogeneous and heterogeneous soil contexts. Overall, the module made it possible to determine changes in soil temperature, monitor the progress of the thaw front, and calculate the depth of the thaw. In this study, the thaw depth of the active layer was an input for the hydrological simulations to calculate the soil moisture, a determining factor in the soil moisture module as mentioned above.

2.4.2. Soil Physical Properties

Global hydrological modeling was adopted for this work, simplifying assumptions such as homogeneous soil properties throughout the catchment area. In terms of vegetation and soil profile, tandem dwarf cedar tree brushes and rockslides (mountain tundra) constitute the predominant landscapes throughout the Kolyma station catchment. They occupy 71% of the land area, compared with 29% of the larch forest [38]. Table 1 shows the physicothermal properties of the soil layer, while the soil profile is shown in Table 2.

Table 1. Soil layer's physical properties.

Soil Layer	Porosity (m^3/m^3)	Density (Kg/m^3)	Heat Capacity (J/Kg °C)	Heat Conductivity (W/m° C)	Maximum Water Holding Capacity (m^3/m^3)
Moss	0.9	500	1930	0.8	0.60
Bedrock	0.35	2610	750	2.3	0.07

Table 2. Soil profile composition.

Depth (cm)	Soil Profile Composition
0–9.99	Moss
10–150	Bedrock

In the study area, the thickness of the active layer rarely exceeds 150 cm. Thus, the composition of the soil profile is given for the first 10 cm, and the rest of the profile, up to the permafrost surface.

2.4.3. Measured Active-Layer Depth

Seasonal thaw depth data have been measured at the Kolyma station since 1954 using Cryopedometers installed in several wells throughout the station. An analysis of the observed data presented in [27] shows that the maximum thaw depth varies from one year to the next and from one site to the next, depending on the vegetation, the local topography, the soil profile, the physical composition of the soil, and the exposure of the site to solar radiation, among others [39]. The thawing process begins in the second half of May and ends in the first half of June. Mountain tundra and cedar tree brush sites have average annual maximum thaw depths of 1.3 m, whereas lower ground with more abundant vegetation has shallow thaw depths (0.6–0.72 m). Since the measurements were not taken directly in the basin shown in Figure 1, the simulated thaw depths were compared with the observed annual average in the western part of the basin, which has the same pattern in terms of vegetation, altitude, and soil profile.

2.5. Integrating Thaw Depth Calculations with HBV

The proposed modeling strategy integrates two independent models, the HBV model and a heat transfer algorithm [22], with the role of calculating thaw depths. The link between the two mentioned models is based on the soil moisture module available in HBV. In the various existing versions of the HBV model, including the one used in the present study [40], simulations are carried out with an initial water content whose value can be adjusted during the calibration process. Following this approach, the appropriate soil moisture value is obtained after several iterations. In fact, of the total precipitation that reaches the ground, only a portion, called the effective precipitation, which is evaluated using Equation (4), contributes to surface runoff, while the other portion infiltrates into the ground.

$$P_{eff} = (P + M)\left(\frac{SM}{FC}\right)^{\beta} \tag{4}$$

Here, P_{eff} is the effective precipitation (mm/d); P is the depth of daily precipitation (mm/d); M is melt (mm/d); soil moisture (SM) is current water content (mm); FC is the field capacity or maximum water content (mm); and β is the shape coefficient. The second term in this equation is the runoff coefficient; it depends directly on the ratio (SM/FC) and the shape coefficient, β, whose value controls the contribution of direct runoff to the watercourse. If the soil's water content and field capacity are known, only the shape coefficient needs to be adjusted during the calibration process. However, when the water content and field capacity are not known (which is often the case), then calibration has to be carried out for these three parameters that determine the runoff coefficient. The standard HBV model, therefore, requires an initial value for water content to trigger the runoff calculation. The initial value of soil moisture is updated according to infiltration and evapotranspiration. Soil moisture is a parameter that changes over time, and one of the strengths of the HBV model is its ability to update parameters throughout the year without stopping the simulation.

To reflect the soil status at the beginning of the warmer period, the current study includes a module that allows the physicothermal properties of the soil to be considered by calculating the advancement of the freeze/thaw front in the soil. We allowed soil storage to increase as the active layer thaws, which is particularly important because runoff is modeled over the course of an entire summer season [41]. The integration of the soil moisture module is facilitated by the link between the water content of the soil and the depth of the active layer, which is limited by the ice layer, which can extend over several hundred meters.

As reported in Refs. [42,43], the total volume (S) of water stored in the active layer thickness (ALT) can be determined using Equation (5):

$$S = AZ_{water} = A\int_0^{ALT} S_d(z)\phi(z)dz \tag{5}$$

where A is the unit area (m^2), Z_{water} is the equivalent height of the water column (m), and dz is the incremental advance of the thaw front in the soil. Also, ϕ and S_d are the porosity and the degree of saturation, respectively, which vary with soil depth (z). Thus, at a known depth, the water content of the soil, θ, can be determined using the degree of saturation and porosity ($\theta = S_d\phi$). The degree of saturation varies between 0 and 1 so that when the soil is saturated, $S_d = 1$ and $\theta = \phi$. One can assume that when snow starts to melt, the thawing front starts to descend as well; the water content in this zone is close to the maximum holding capacity, and the thawed soil is saturated. During the snowmelt period, evaporation is not significant when compared to the extraordinary supply of meltwater to the thinly thawed active layer [44]. Equation (6) then leads to the relationship establishing the link between the equivalent height of water and the thaw depth for a unit surface area:

$$Z_{water} = \phi z \tag{6}$$

Thus, calculating the thaw depth using the algorithm mentioned in Section 2.3 feeds the soil moisture module according to the modeling structure shown in Figure 2.

To calculate the water content present in the soil (SM), rainfall is added to the water content that already exists in the soil, and then the effective rainfall, i.e., runoff and evaporation, is subtracted according to the following relationship:

$$SM = Z_{water} + lwater - Peff - Ea \tag{7}$$

where $lwater$ is the liquid water (rainfall), and Ea is the actual evapotranspiration.

The link between the heat transfer module and the HBV model forms a model named HBV-Heat in the current study. This model is implemented under Matlab, and its application to the Kontaktovy basin forms the basis for the results presented in the next section.

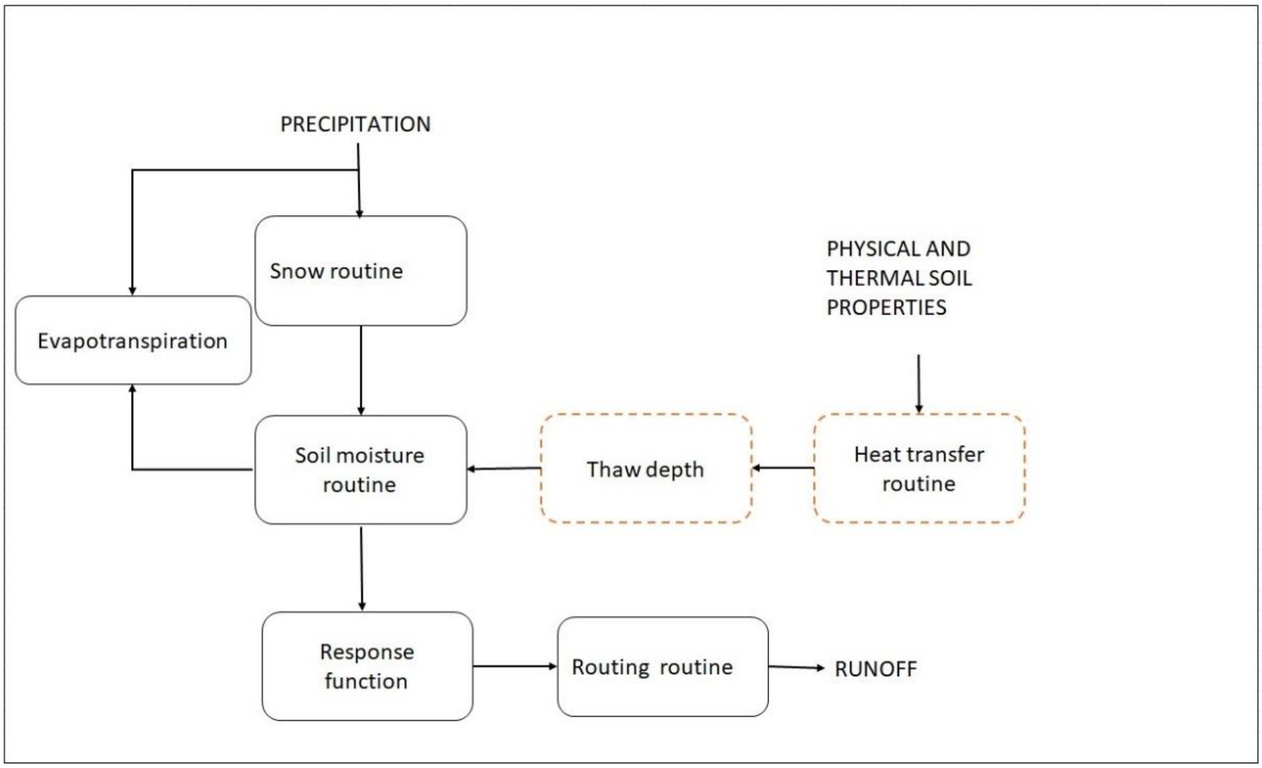

Figure 2. Structure of the applied model.

2.6. Model Calibration

The calibration of the proposed model was performed by comparing the observed and simulated discharge at the outlet of the watershed during the period 1960–1965. For that, model parameters (Table 6) were iteratively adjusted manually to minimize disagreements between the predicted and measured hydrographs. The whole calibration process was based on visual inspections of the hydrographs, and the Nash–Sutcliffe efficiency index (NSE) was used as the objective function, as presented in Table 3 [45].

Table 3. Statistics.

Error Measures	Description	Range
Nash–Sutcliffe Percent bias	$NSE = 1 - \frac{\sum_{i=1}^{n}(Q_{obs}-Q_{sim})^2}{\sum_{i=1}^{n}(Q_{obs}-\overline{Q_{obs}})^2}$ $PBIAS = 100\,\frac{\sum_{i=1}^{n}(Q_{sim}-Q_{obs})}{\sum_{i=1}^{n}(Q_{obs})}$	$-\infty < NSE < 1$ $-\infty < PBIAS < +\infty$
Root mean squared error	$RMSE = \sqrt{\frac{\sum_{i=1}^{n}(Q_{sim}-Q_{obs})^2}{n}}$	$0 \leq RMSE < +\infty$

Note: where Q_{obs} is the observed discharge (m³/s); Q_{sim} is the simulated discharge (m^3/s); and $\overline{Q_{obs}}$ is the average of the observed discharge (m^3/s).

The NSE ranges from $-\infty$ to 1; when the NSE equals 1, it means there is a perfect match between the observed and the predicted hydrographs (error variance equals 0.0). Conversely, an efficiency value smaller than or equal to 0.0 indicates that the proposed model is no better than using the baseline model [46]. In addition to the above criteria, the calculated values of evapotranspiration, snow water equivalent (SWE), and soil moisture (SM) aided in the calibration process, especially when comparing the proposed model and the HBV model. Table 3 shows the error measures used in conjunction with the performance index for their informative values.

The percent bias (PBIAS) is expressed as a percentage and measures the average tendency of the simulated data to be greater or smaller than the observed data. The optimal value of PBIAS is 0.0, with low-magnitude values indicating that the model is accurate. Positive values indicate model underestimation bias, whereas negative values are interpreted as indicating model overestimation bias [47].

The root mean squared error (RMSE) measures the difference between the predicted values obtained by the model and the actual observed values. Values close to 0.0 indicate a perfect fit, with values smaller than half of the standard deviation of the observed values being considered low [48].

2.7. Model Validation

The validation of the proposed model was performed with an independent time series (1977–1981); the optimal parameters obtained during the calibration step were used without adjusting their values. The same metrics used before were evaluated.

3. Results

In this section, the results of the proposed thaw depth model are presented, and the figures illustrating the advancing thaw front are provided in Appendix C (Figures A7–A12). The hydrological response of the Kontakovy Creek catchment was investigated from a number of perspectives. First, the HBV model and the HBV-heat model were compared for the years 1960 to 1965. In particular, this comparison showed how the inclusion of the heat transfer module affected the discharge. The simulated hydrographs for the calibration and validation periods were then compared with the observed data.

3.1. Simulated Thaw Depth

The simulated thaw depth data for the calibration years are shown in Table 4. It should be noted that heat transfer does not require calibration. Although no observations are available for the basin under consideration, the results obtained were nevertheless compared with the observed average at measurement point #2 as defined in [26] at the meteorological plot Verknyaya, located at 1261 m.a.s.l. and with coordinates of (61.8574 N; 147.611 E). Due to the lack of data for the validation period (1977–1981), only the calibration period (1960–1965) could be compared. Note that the maximum yearly depth observed between 1954 and 1966 was 128 cm [30].

Table 4. Simulated thaw depth.

Year	Thaw Depth (cm)	
	Simulated	Measured
1960	129.70	>120
1961	132.16	-
1962	132.28	-
1963	128.57	136
1964	126.72	126
1965	129.04	131
Average	129.75	-

The average of the simulated depths of thaw for the period is similar to the average reported in [30], with a difference of about 1.5%. This implies that the model can simulate the maximum thawing depth of a multilayer soil with a high degree of accuracy. These results are also in line with those published in [22], based on simulations carried out for soil profiles from different landscapes that dominate the KWBS. The advance of the thaw front is illustrated for each of the simulated years in the graphs presented in the Appendix C. In general, these graphs show that the annual maximum is reached in August and that the ground is completely frozen by October. A comparison of the simulated years shows that the maximum depth of thaw was reached in 1962. An examination of the soil temperatures for this year shows that the average temperature for the period from 10 May to 15 September was 10.4 °C, which was 5% higher than the observed average for the simulated period. The year 1964 had the lowest simulated thaw depth of 127 cm, while its average temperature was 4% lower than the average for the considered period. The results are consistent from this point of view because the solution of the heat transfer equation in porous media involves boundary conditions, especially temperature. The direct use of soil temperature instead of air temperature reduces the error that could be associated with the application of any approximation method. In fact, during heat transfer, heat is moved by the temperature difference between the soil surface and the underlying permafrost layer. The use of air temperature instead of soil temperature may lead to inaccurate estimates of permafrost thawing and its effects, as it may not adequately reflect the temperature gradient causing heat transfer. Furthermore, as air temperature can be affected by variables such as wind, precipitation, and cloud cover, ground temperature measurements are often more accurate.

The calculated depths can, therefore, be used as an input to determine soil moisture, upon which evaporation and surface runoff depend.

3.2. Proposed Model

The optimal parameters obtained using the HBV-Heat model were compared to the parameters obtained using the HBV model. The results of the comparison are shown in Table 5 in terms of the NSE obtained for each year; the model parameters are shown in Table 6, and the definition of each parameter is provided in Appendix A (Table A1). It can be seen that, on average, the HBV-Heat model provides the best results for the period with the highest hydrological activity during the year. There is a 30% improvement in the overall results achieved compared to the existing HBV model.

Table 5. Comparison between the HBV model and HBV-Heat model based on NSE statistics.

Model	**NSE**						
	1960	**1961**	**1962**	**1963**	**1964**	**1965**	**Average**
HBV	0.66	0.49	0.54	0.74	0.08	0.46	0.50
HBV-Heat	0.59	0.62	0.72	0.77	0.57	0.62	0.65

Table 6. Model parameters.

Parameters	**DD**	**FC**	**Beta**	**C**	**L**	**K_0**	**K_1**	**K_2**	**K_P**	**TT**
Values	1.06	156.9	0.21	0.79	70.2	0.79	0.33	0.11	0.20	1.20

Figure 3 shows the difference between the measured discharge values and those calculated by the existing and proposed models. For the considered period, 1964 had the lowest NSE. In view of the results, the HBV-Heat model was used with confidence to simulate the various components related to the water balance of the Kontaktovy stream basin.

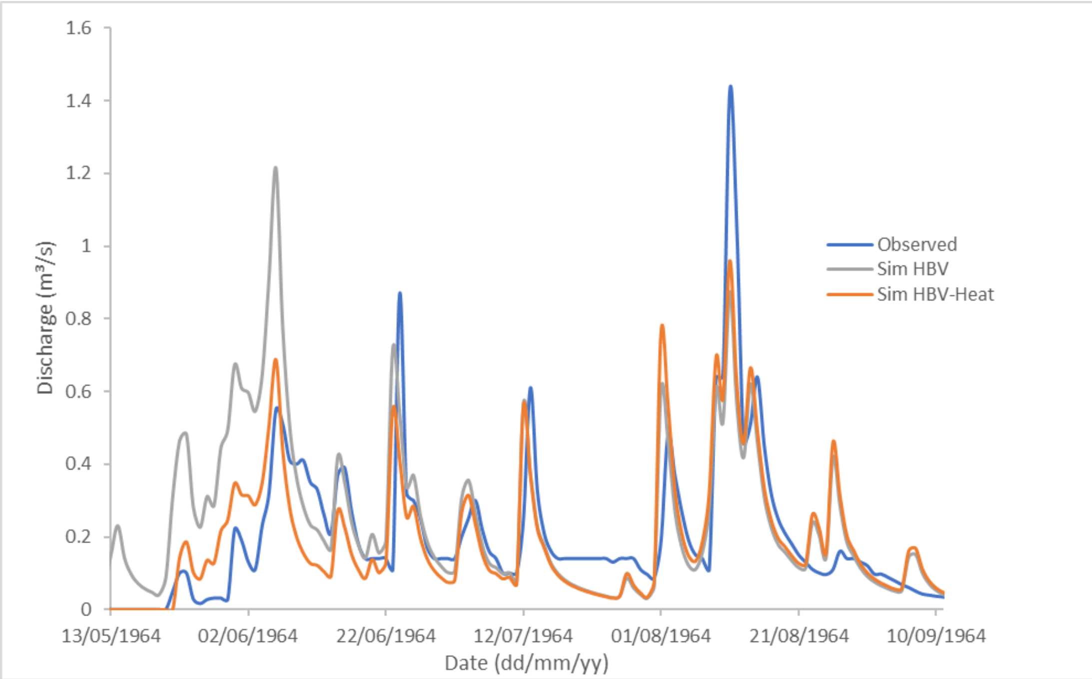

Figure 3. Simulated hydrographs based on HBV and HBV-Heat in respect of observed hydrograph (1964).

3.3. Simulated Hydrographs for the Calibration and Validation Periods

Based on continuous simulation for both the calibration and validation periods, Figures 4 and 5 show the comparison of the simulated and observed hydrographs obtained for the two periods.

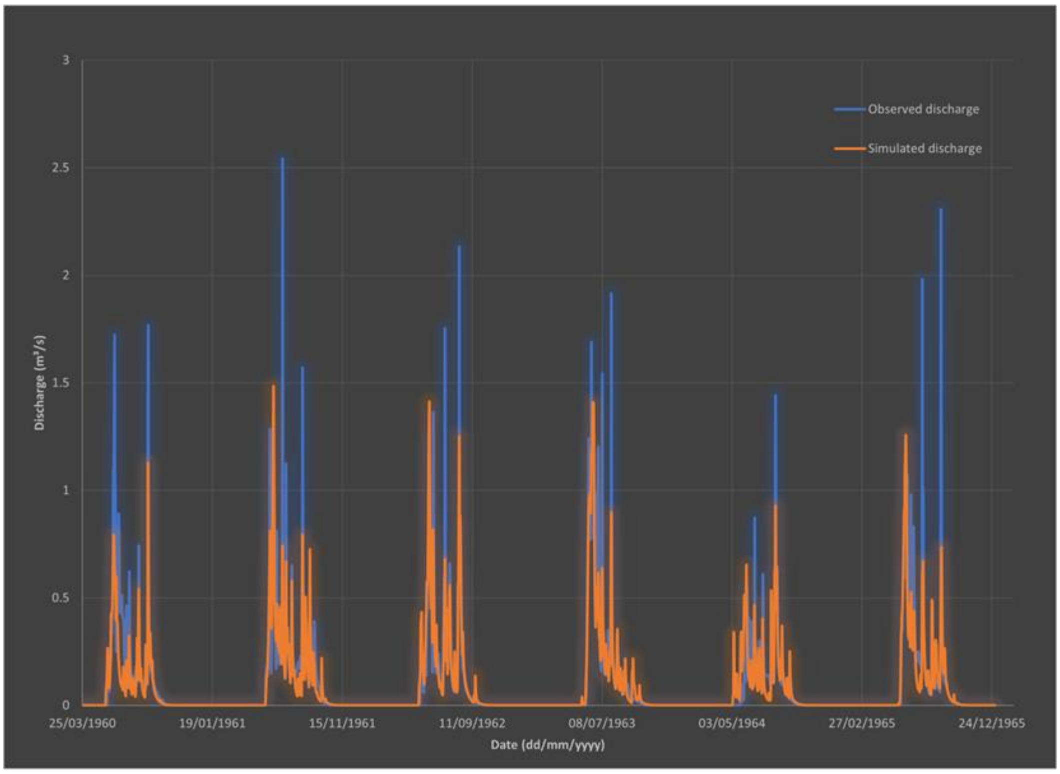

Figure 4. Observed and simulated discharges for the calibration period (1960–1965).

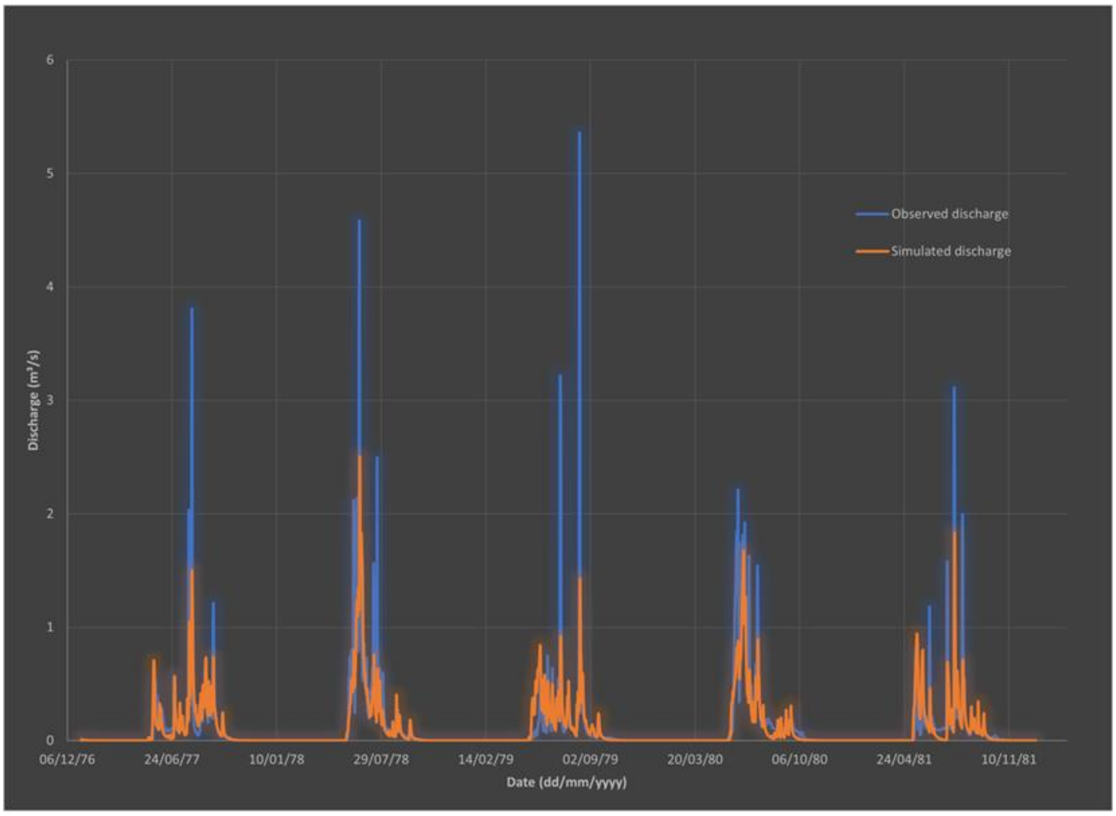

Figure 5. Observed and simulated discharges for the validation period (1977–1981).

The visual analysis first allowed a rough assessment of the quality of the calibration (Figure 3), and then the statistical criteria were used as indicators to determine the robustness of the proposed model. It can be seen from the figures that the proposed model reproduces the measured flow with very good accuracy, resulting in an overall efficiency of 0.74 (NSE). This means that the model can capture not only the time of occurrence but also the magnitude of peak flows. While most small flows are satisfactorily reproduced, peak flows are sometimes underestimated both in late spring and in summer, especially during rainfall events. From a yearly point of view, the years 1962 and 1963 are the best in terms of the model's ability to reproduce the timing of the peak flow, low flow, and total amount of flow generated. However, the year 1964, as shown in Appendix B (Figure A5), shows a discrepancy mainly in terms of the time of occurrence and the volume of the peak flow. Despite this weakness in the model, the PBIAS calculated at the end of the calibration period is acceptable (see Table 7). This statistical criterion makes it possible to measure the percentage error between the simulated and measured values, with an emphasis on the volumetric error in the flow simulation. However, for the validation period, the statistics are weaker, as can be seen in Table 7. The results show that the different metrics either decreased or increased during the validation process. The NSE decreased by 36%, while the PBIAS and RMSE increased by 100% and 24%, respectively. This overall decrease in performance can be explained by the fact that the two analyzed periods show differences in terms of the inputs used. For example, the sum of precipitation for the entire calibration period was 13% lower than that for the validation period, while the average flow for the two periods was almost the same, i.e., 0.26 m^3/s. This inconsistency is due to the way the data were collected. As the two periods were separated by 13 years, it can be assumed that there had been a technological change in the intervening period. This implies that replacing old measuring equipment led to differences in the quality of field measurements. A sensitivity analysis of the various parameters was carried out to determine which parameters had the greatest influence on the efficiency of the proposed model. By varying one parameter at a time and keeping the others constant, the degree-day factor was found to be the most sensitive. The efficiency of the model (NSE) increased from 0.3 to 0.6 when the iterations were carried out in the range of values between 1 and 3. The optimal value for all simulations was 1.3. The other influential parameter was the recession constant of the upper reservoir, with an optimal value of 0.3 being maintained throughout the optimization procedure.

Table 7. Model efficiency for the calibration and validation periods.

Period	Years	Goodness of Fit		
		NSE	RMSE	PBIAS
Calibration	1960–1964	0.74	0.12	−11.6
Validation	1977–1981	0.55	0.24	−14.4

3.4. Simulated Snowmelt

The HBV model's snow routine applies the temperature-index approach to snowmelt modeling following Equation (8):

$$M = DD\ (T_m - TT) \tag{8}$$

where M is the snowmelt rate as SWE (mm/day); DD is the degree-day factor (mm/°C·day); T_m is the mean daily air temperature (°C); and TT is the threshold value of temperature (°C).

An illustration of the simulated SWE is provided in Figure 6 for the year 1961. Snow accumulation begins in September while melting starts in May. Over the simulated period from 1960 to 1965, snowmelt began at the earliest on May 3 and ended at the latest on June 21, lasting between 3 and 4 weeks. The simulated values of the SWE are presented in Table 8, alongside the measured values reported in [30] for the data obtained from the station KWBS_runoff_1102 (latitude of 61.85; longitude of 147.65). It should be mentioned that the SWE values presented by the aforementioned authors were obtained by transforming measured snow heights using Equation (9).

$$SWE = h_s \times 10 \times \frac{\rho_s}{\rho_w} \tag{9}$$

where h_s represents the measured snow depth (cm), while ρ_s and ρ_w are the snow and water density (kg/m^3), respectively, for the SWE (mm). With the exception of 1960, when the model underestimated the observed value by around 54%, in general, the model generated SWE values that were fairly close in order of magnitude to those observed for the other years. The differences between the simulated and observed values varied between −7.5% and +13%, with the years 1964 and 1965 showing the smallest difference, i.e., an overestimate of 3%. Given the simplicity of the calculation method, the results obtained are acceptable. Through the calibration process, the parameters used to simulate snowmelt, namely the threshold temperature (TT) and the melting factor (DD), were determined to be equal to 1.2 °C and 1.3 mm/°C, respectively.

Table 8. Observed and calculated snow water equivalent.

Year	SWE (mm)	
	Observed	Simulated
1960	114	62
1961	113	121
1962	120	111
1963	122	139
1964	59	61
1965	119	123

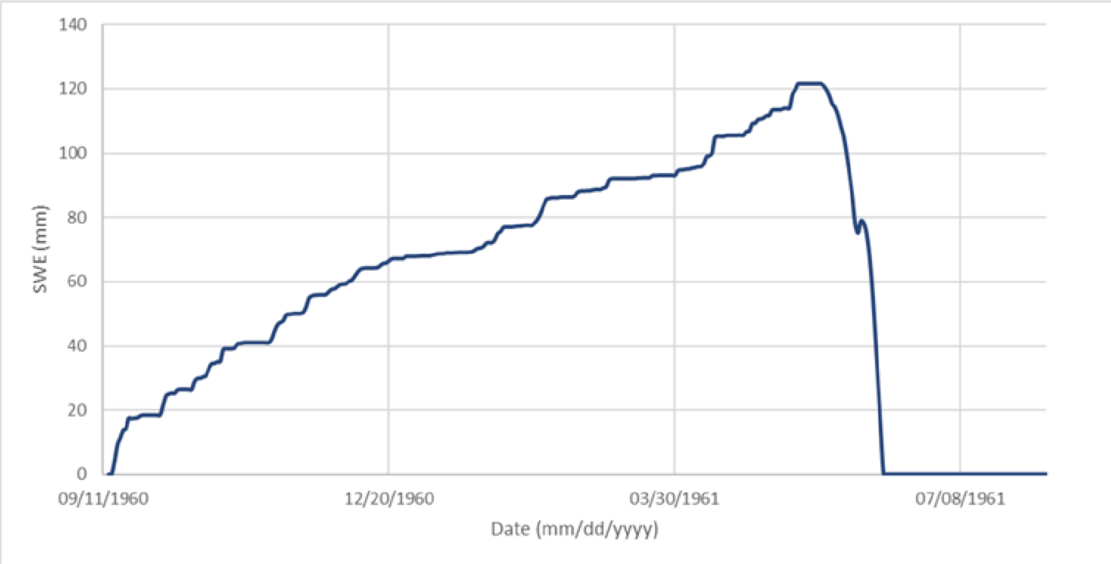

Figure 6. Simulated SWE (1961).

3.5. Evaporation

Evaporation is an important parameter for calculating the water balance of a watershed, but it is not always easy to determine, especially in permafrost conditions due to the low evaporation rate and the frozen ground. Our model was used to simulate this phenomenon, and the results are shown in Figure 7. The model was fed with long-term monthly evaporation data obtained for the period from 1972 to 1990, and subsequently, daily evaporation was simulated. The average calculated evaporation for the calibration period was 162 mm, while the maximum and minimum values were 185 and 113 mm, respectively. The model was only able to calculate evaporation that took place during the warm season between May and September. It is worth mentioning that evaporation during a hydrological year under KWBS conditions is composed of not only the sublimation of the snow cover during the cold period but also evaporation from both snow and the ground during the transition period, due to an unevenly distributed snow cover [49]. An analysis of evaporation in relation to the mean temperature recorded during the calibration period shows that the years 1960 and 1961 had almost the same mean temperature, at 9.1 and 9 °C, respectively. Their annual evaporation was also the same, at 179 mm. The year 1962 had the highest annual evaporation of 185 mm, and the corresponding mean temperature was 9.9 °C, which was the maximum mean temperature for the period of 1960–1965.

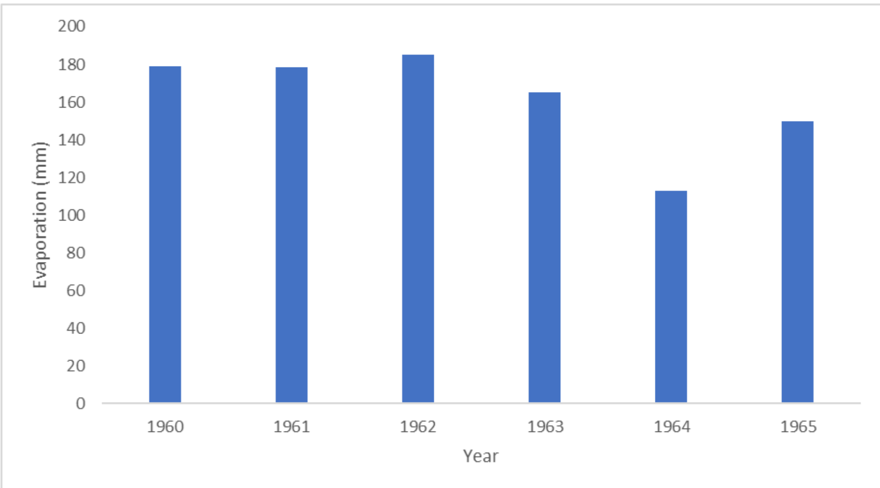

Figure 7. Calculated evaporation for the years 1960–1965.

3.6. Calculated Soil Moisture

The results of soil moisture for each year show that it varies due to climatic conditions, which determine the soil water history at the beginning and end of each hydrological year.

Figure 8 illustrates the variation in water content in the soil during the warm period of the year 1963, showing an initial peak just after the snow melted and other peaks following the summer rains. Between two rain events, there is a period of recession during which the water equivalent in the soil likely decreases due to runoff into watercourses and evapotranspiration. The latter process is controlled by plant type, soil texture, and the biophysical properties of vegetation [50]. In 1963, after the snow had melted, the water in the modeled reservoirs reached 35 mm. During the course of the season, this quantity fluctuated considerably as a result of rain, which increased its content, and in the absence of direct input, a net decrease was observed.

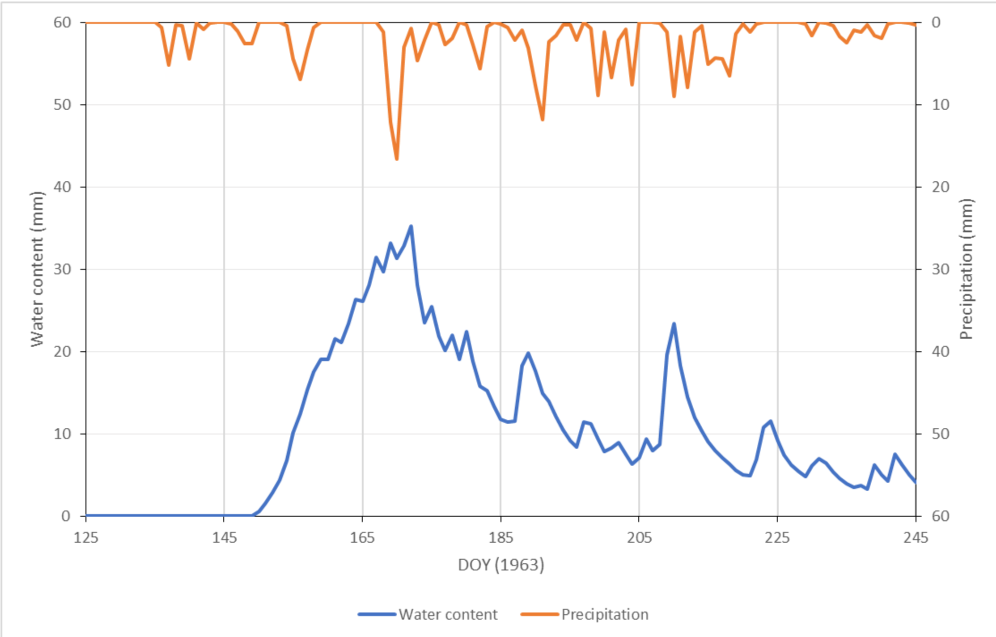

Figure 8. Soil water content variability in 1963.

3.7. Water Balance

All the elements analyzed in the precedent sections facilitated the establishment of the water balance of the basin for the period of 1960–1965. Note that the general relationship (Equation (10)) was used for the warm season of the year, i.e., between 1 May and 15 September, without adjusting the precipitation values.

$$P + SWE - R - Ea = \eta \tag{10}$$

Here, P, SWE, R, and Ea represent liquid precipitation (mm), snowmelt water equivalent (mm), surface runoff (mm), and evaporation (mm), respectively, and η represents the residual (storage and error due to measurement uncertainty, in mm). The snowmelt water equivalent was obtained between 1 May and the time of the spring freshet, as mentioned in Section 3.4. The precipitation used to calculate the water balance is the sum of the precipitation that fell between the start of snowmelt and mid-September, while evapotranspiration is the sum of the daily values for the entire warm period. Surface runoff is the cumulative value of runoff between the start of snowmelt and refreezing.

The simulated water balance components for the six years considered in this analysis are shown in Figure 9. From the figure, we can see that the residual is negative only for the year 1964, whereas it is positive for the other years. This negative residual can be explained by the low rainfall recorded that year. Indeed, compared with other years, the measured rainfall was 13% lower than the average for the entire period under consideration. At the same time, we know that in the short term, soil infiltration conditions do not change significantly unless an unusual event such as a forest fire occurs during the year. With all other things being equal, the flow/rainfall (Q/P) ratio and evaporation values remain similar to those of previous years. In this context, the application of Equation (4) produces a residual smaller than 0. In explaining the negative residual values obtained when calculating the water balance of the KWBS for the period of 1970–1985, [49] stated that, "*The negative values of discrepancies indicate the presence of moisture not taken into account that was formed by transient water storage in snow and also by ice in the strata of talus deposits*".

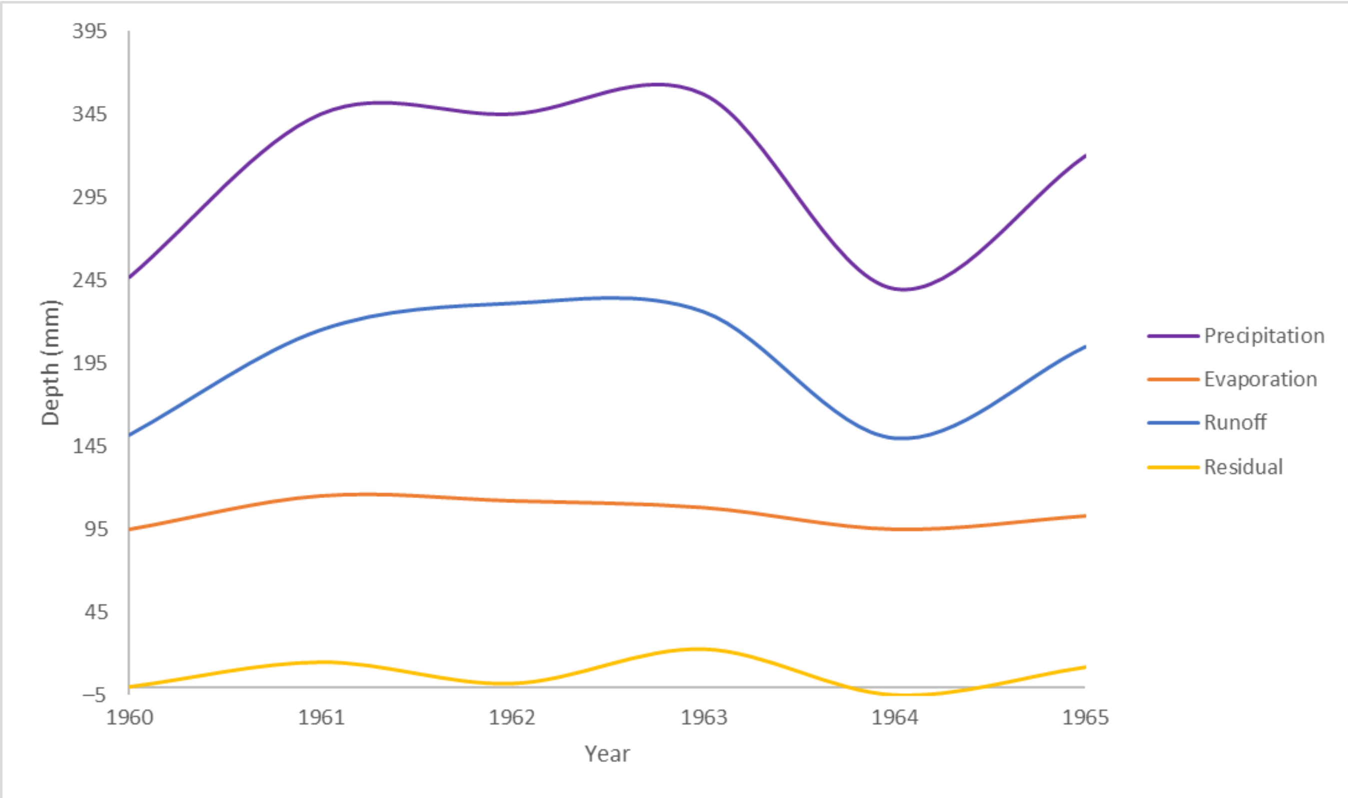

Figure 9. Simulated annual water balance.

When we compared the (Q/P) ratios with those calculated by [49] for a larger basin (21.4 km^2), including our study area, we found that our values are lower in order of magnitude. Our values reach an average of 64%, while the values reported by those authors reach an average of 73% for the period of 1970–1985. However, for a small headwater (Severny; area = 0.38 km^2), the average ratio is closer to 56% for the period of 1958–1997 [51]. Overall, the presented results demonstrate that the water basin is characterized by low precipitation, relatively low evaporation, and high runoff. This finding is in line with what has been asserted in [30,49].

4. Discussion

The heat transfer module integrated into the model proposed in the present study allows physical characterization that improves the model's estimation of the components of water balance. However, it should be noted that the mathematical equations representing the different processes involved in the hydrological response of the basin are simplified. Nevertheless, from the runoff generation point of view, for both the proposed model (HBV-Heat) and the physical model used in previous studies on the Kolyma water-balance station (KWBS) basin, especially the hydrograph model [52], the reservoir concept used for simulating soil moisture remains the same. Therefore, it is reasonable to compare the results obtained by the proposed model with those of previous studies, even though the analyzed periods and the areas of the basins are different. Both similarities and dissimilarities were examined to demonstrate the relevance of the proposed modeling approach. It should be noted that the developed model, despite its simplicity, produced results showing the same trend as those of [27] with respect to runoff. These authors found that, during the summer period, runoff consists mainly of subsurface runoff and a small amount of surface water, which is mainly from rainfall events. Indeed, the finding that more water comes from the subsurface can also be explained by the fact that the investigated soil layers have different porosities, including a value of 0.9 for the upper layer and a value of 0.35 for the lower layer. The soil is, therefore, more permeable in the root zone, which is made up of organic matter and humus, whose decomposition creates spaces in the soil that ultimately facilitate the movement of water. The upper layer, therefore, allows more water to pass through the lower reservoir. Then, this water is trapped between the ice layer and the soil surface. This configuration allows the trapped water to feed the flow measured in the tributary stream quickly and in large quantities. It is worth mentioning that, compared to the results calculated by the proposed model, the results of the occurrence of peak flows and their magnitude, as well as the recession of the hydrograph after rainfall, obtained using the model presented in [53], underestimate the observed summer peaks. The authors explained this underestimation by the fact that their model does not account for the fact that not enough water is stored in the ground during the snowmelt period to be used later. In addition, the hydrograph shows a rapid retreat after rainfall so that the base flow returns to zero, similar to what occurs in October and May. However, using the HBV-Heat model, the flow does not drop to zero throughout the warm period, and most of the flows are simulated satisfactorily, either in terms of the timing of their peaks or their values. This implies that the heat transfer module, which calculates the daily thaw depth, ensures that the ground is supplied with water on a daily basis, allowing the base flow to be simulated satisfactorily because water from the thaw is always available. It should be noted that the HBV-Heat model slightly overestimates the peak discharge just after snowmelt. This is because water from the snowmelt cannot fully infiltrate into the ground, which is still frozen to a great depth, so there is more surface runoff. This behavior is also reported in [54], particularly for the larch forest that is part of the study area. It is indicated in [41] that infiltration is not fully captured by the model, which explains the difficulty in obtaining a better fit based on observations at the very beginning of the warm season. With regard to the simulated snow water equivalent, despite the use of the simple degree-day (DD) method and the neglect of the snow damming phenomenon, the model is able to satisfactorily predict the SWE obtained from the snow data for the whole period, except for the year 1960, which was underestimated by 54%. It should be noted that the proposed model does not include a runoff routing function, as is the case with other versions of the HBV model. In fact, this function compensates to a certain extent for the fact that the phenomenon of snow damming is not considered since it is linked to the distribution of snow and possible avalanches in mountainous areas, as is the case for the studied basin in [55]. The proposed HBV-Heat model also makes it possible to estimate actual evaporation in the catchment using a simple relationship that links evaporation to the soil water content. In general, actual evaporation is lower than potential evaporation because the soil water content is below the permanent wilting point. It should also be noted that the field capacity (FC) and permanent wilting point (PWP) are physically based parameters that needed to be calibrated because no field values were available. In this context, a comparison of the HBV-Heat model with the existing model (HBV) in terms of optimizing flow and evaporation shows that the ratio of actual evaporation to potential evaporation (Ea/Ep) of the proposed model is 16 times greater than that of the existing model. This difference implies an improvement in the calculation of actual evaporation, which includes evaporation from soils, plants, and water bodies. As a result, the heat transfer module provides an input that subsequently enables a more realistic calculation of evaporation and runoff. The calculated water balance is in the same order of magnitude as that obtained for the large KBWS basin by [51] over a longer period (1949–1990). However, an analysis of the average discharge over this period (197 mm) shows that it is still low compared to the discharge of 296 mm reported in [49] for the period of 1970–1985. So, there is still a problem regarding the accuracy of the incoming data, regardless of whether it is precipitation, runoff, or evaporation data. Ref. [56] stated that calculating the components of the water balance is very complicated and subjective, even when data are available. It should also be noted that the global modeling approach used in this study does not reduce the errors associated with the input data, as the model does not consider the orographic effect, which exists in basins where the difference in elevation is significant.

5. Conclusions

Modeling the hydrological response of a basin located in a continuous permafrost environment is a complex and essential activity in the assessment of water resources and the construction of infrastructures. The seasonal freeze–thaw phenomenon, upon which the hydrological activity throughout the year largely depends, deserves special attention due to its role in infiltration. In this context, a model integrating a heat transfer module in porous media with a rainfall-transformation model, named the HBV-Heat model, was proposed to assess the different components of the water balance of a sub-basin of the Kantaktovy Creek, located in Eastern Siberia, Russia.

The thaw depth was simulated for each year between 1960 and 1965, with the results showing that the average maximum annual depth for the study period was 1.30 m. These results are in line with those published in previous studies [22,26,57].

Considering the optimized parameters of the model, in particular the components of the water balance (streamflow, evapotranspiration, and SWE), the proposed model performed better than the HBV model, with a Nash–Sutcliffe efficiency (NSE) of 0.74 compared to 0.54 over the entire analysis period. The model calibrated for the period 1960–1965 was used for validation for the period 1977–1981. The proposed model was used in further analyses, although efficiency was reduced by 31% due to differences in the quality of the used inputs.

In terms of the water balance components, the obtained results do not differ significantly from the observed or simulated values reported in previous studies. It was found that, in this catchment, surface runoff or effective precipitation represented 64% of the observed precipitation (rain and snow). The simulated snow water equivalent (SWE) was compared with the observed values obtained from the conversion of snow depth, and it was found that they were of the same magnitude.

Evapotranspiration was the most difficult component to assess, given the quality of the available data. Comparing the results of the period of 1960–1965, the calculated values were overestimated by 29% compared to the observed values for the same period. When the comparison was over a longer period (1949–1990), the calculated results were underestimated by 30% compared to the observed values.

With the heat transfer module, it is possible to use the model proposed in the present study as a tool for analyzing the components of water balance to maintain the base flow at a non-zero level during the warm period, thus improving the surface runoff simulation. The novelty of this study can be seen in the modeling approach put forward, which enables an existing conceptual model to integrate both the physical and thermal properties of the soil.

However, it should be noted that modifications to the snow module of the rainfall-runoff transformation model are necessary to improve the results, in particular by including functions that are capable of analyzing snow damming, which is an important phenomenon in the distribution of snow in sub-Arctic regions.

Author Contributions: Conceptualization, A.L.T.; methodology, A.L.T.; software, A.L.T.; validation, A.L.T.; formal analysis, A.L.T.; investigation, A.L.T.; resources, A.L.T.; data curation, A.L.T.; writing—original draft preparation, A.L.T.; writing—review and editing, A.L.T. and M.F.; visualization, A.L.T. and M.F.; supervision, M.F.; project administration, M.F.; funding acquisition, M.F. All authors have read and agreed to the published version of the manuscript.

Funding: This research received no external funding.

Data Availability Statement: The data supporting the reported results can be found at "PANGAEA. Data Publisher for Earth and Environmental Science" (see Makarieva et al., 2017 [37]).

Acknowledgments: We would like to thank Arman Rokhzadi for reviewing this manuscript. We are also thankful to the anonymous reviewers who took their time reading this manuscript and formulating comments that helped improve the paper.

Conflicts of Interest: The authors declare no conflicts of interest.

Appendix A. Model Parameters

Table A1. Model parameters used in the calibration process.

Parameters	Explanation
TT	Threshold temperature
DD	Degree-day factor
PWP	Permanent wilting point
FC	Field capacity
L	Threshold water level
BETA	Shape coefficient
C	Correction factor for potential evaporation
K_0	Near-surface flow storage
K_1	Interflow storage coefficient
K_2	Baseflow storage coefficient
K_P	Percolation storage coefficient

Appendix B. Hydrographs from 1960 to 1965

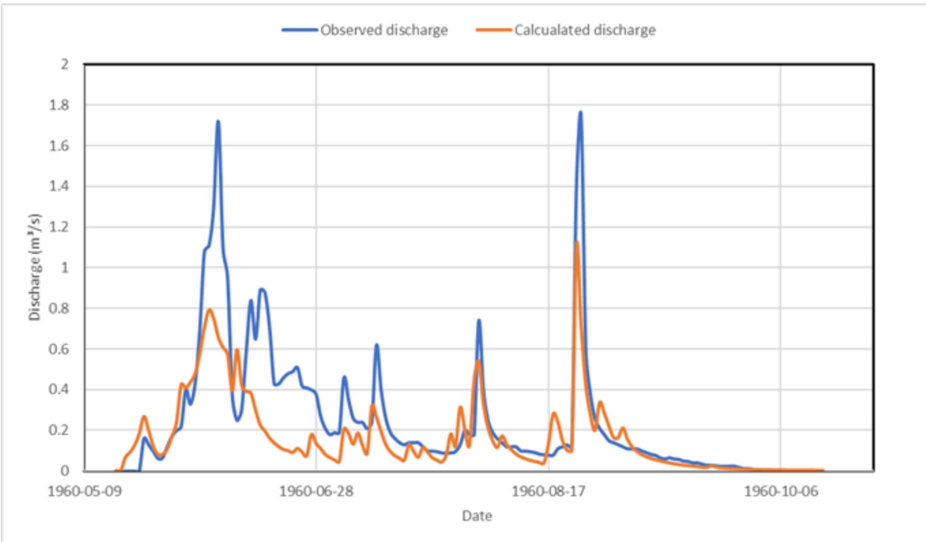

Figure A1. Observed and simulated hydrographs (1960).

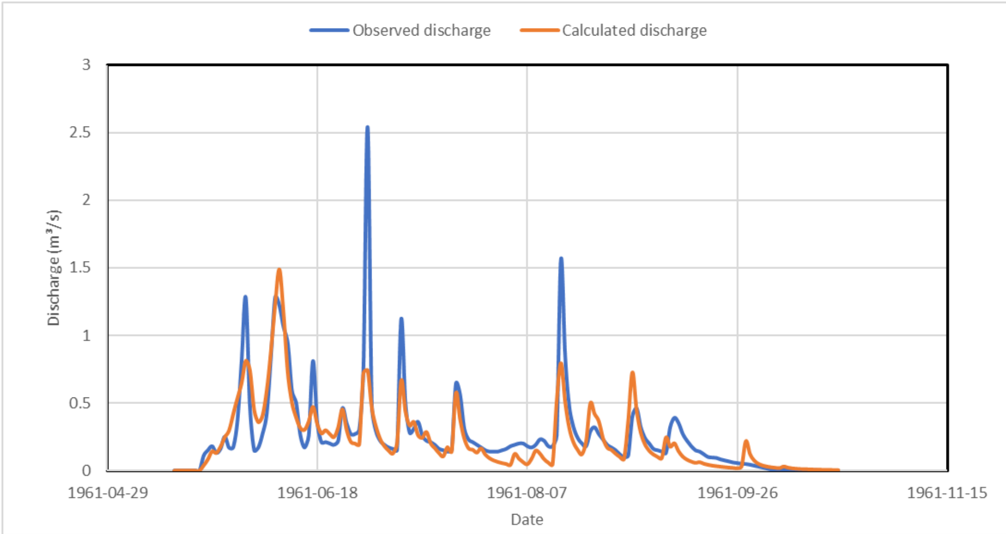

Figure A2. Observed and simulated hydrographs (1961).

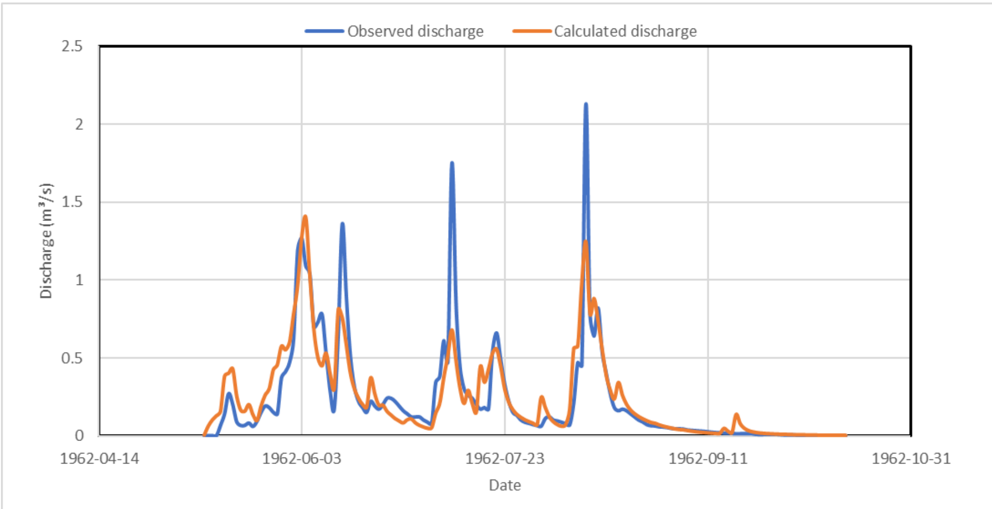

Figure A3. Observed and simulated hydrographs (1962).

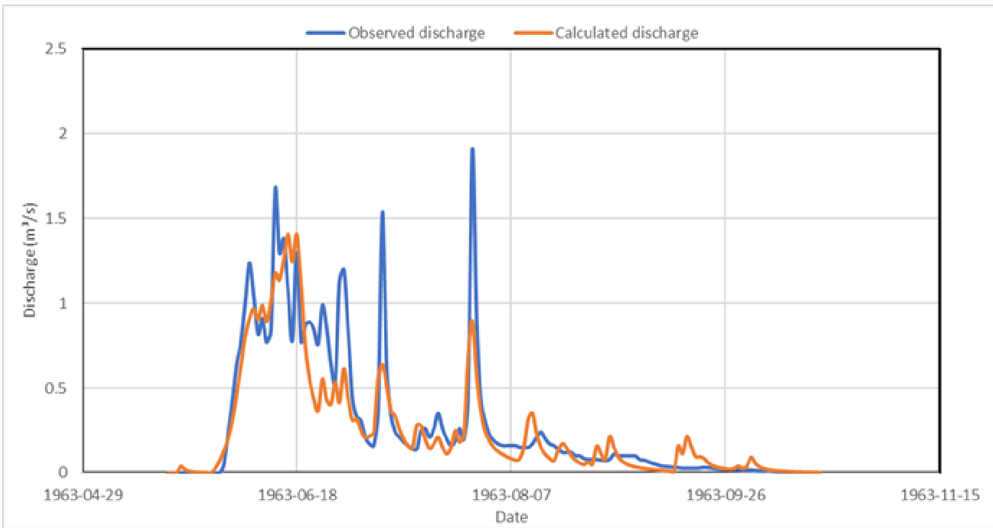

Figure A4. Observed and simulated hydrographs (1963).

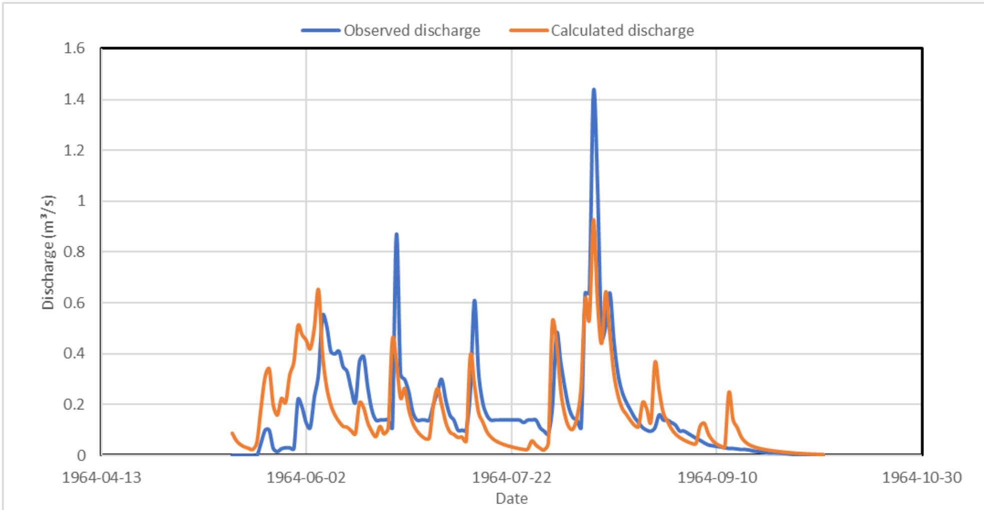

Figure A5. Observed and simulated hydrographs (1964).

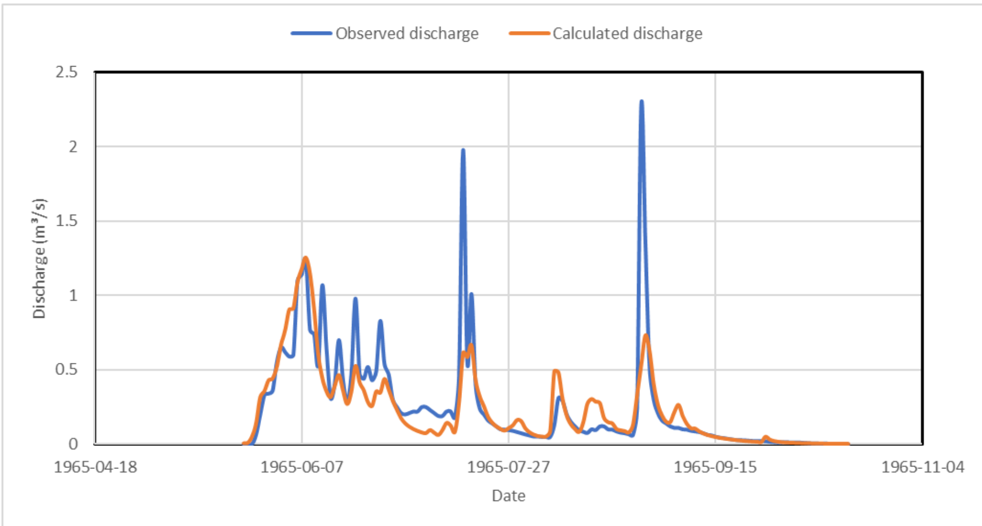

Figure A6. Observed and simulated hydrographs (1965).

Appendix C. Simulated Thaw Depths

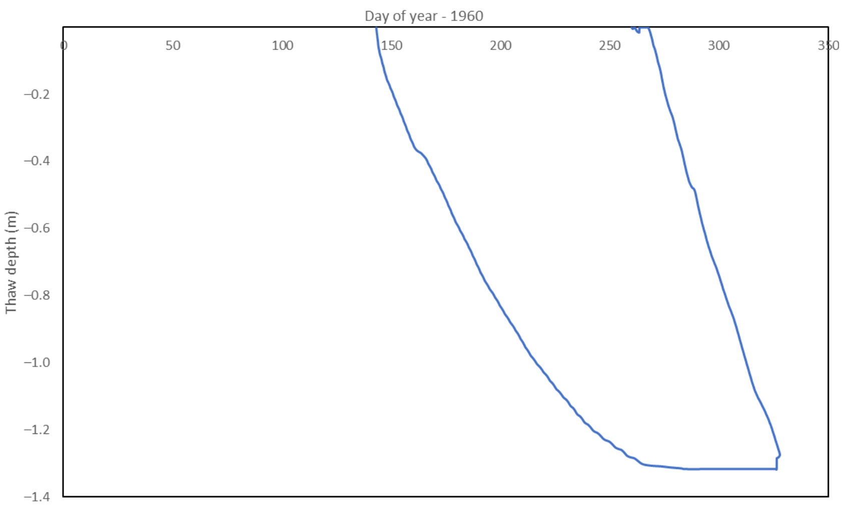

Figure A7. Simulated thaw depth (1960).

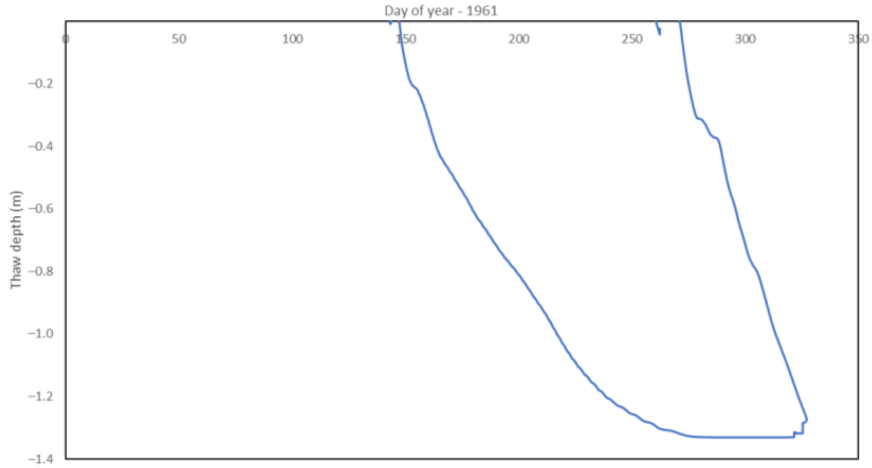

Figure A8. Simulated thaw depth (1961).

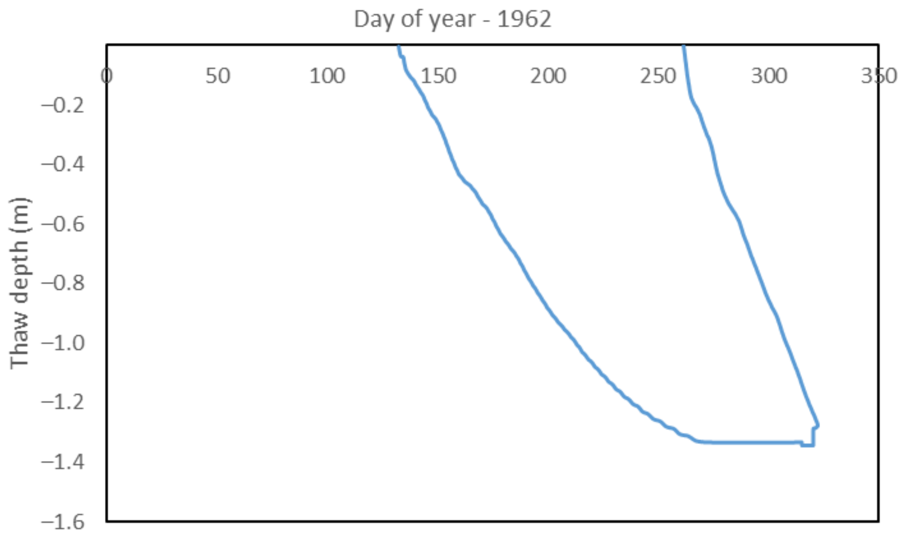

Figure A9. Simulated thaw depth (1962).

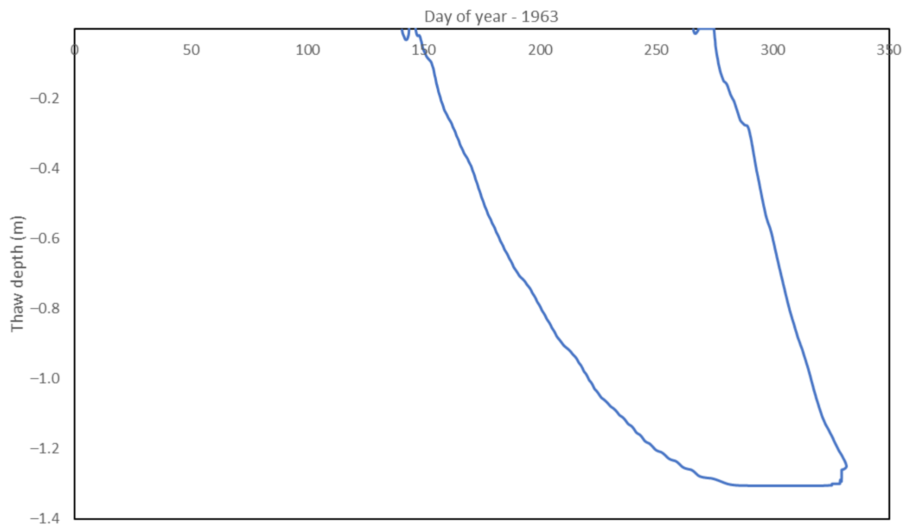

Figure A10. Simulated thaw depth (1963).

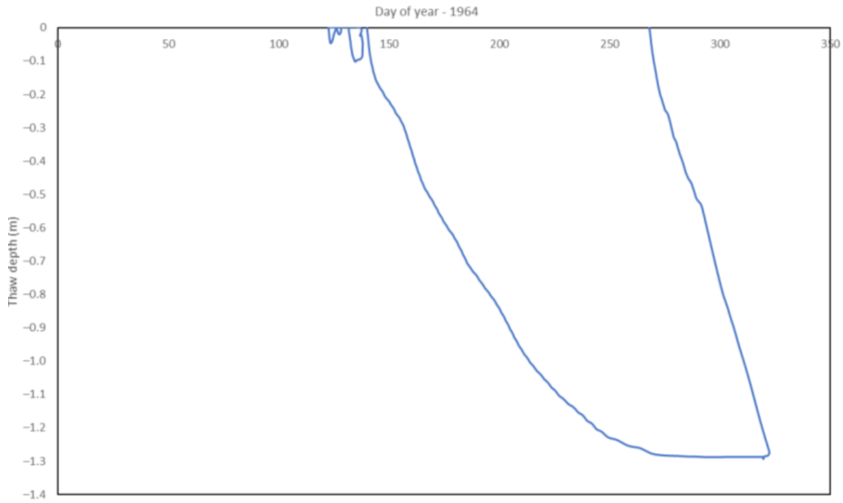

Figure A11. Simulated thaw depth (1964).

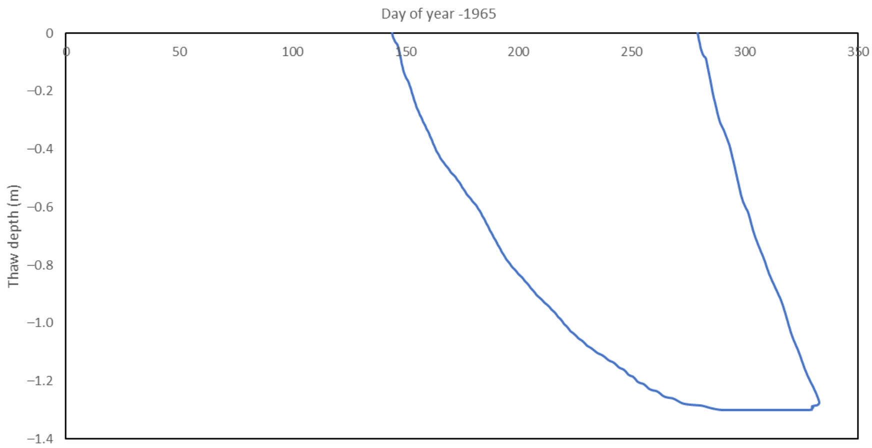

Figure A12. Simulated thaw depth (1965).

References

1. Painter, S.L.; Coon, E.T.; Atchley, A.L.; Berndt, M.; Garimella, R.; Moulton, J.D.; Svyatskiy, D.; Wilson, C.J. Integrated surface/subsurface permafrost thermal hydrology: Model formulation and proof-of-concept simulations. *Water Resour. Res.* **2016**, *52*, 6062–6077. [CrossRef]
2. Woo, M. Permafrost hydrology in North America. *Atmos. Ocean* **1986**, *24*, 201–234. [CrossRef]
3. Zhao, L.; Gray, D.M. A parametric expression for estimating infiltration into frozen soils. *Hydrol. Process* **1997**, *11*, 1761–1775. [CrossRef]
4. Gao, H.; Wang, J.; Yang, Y.; Pan, X.; Ding, Y.; Duan, Z. Permafrost Hydrology of the Qinghai-Tibet Plateau: A Review of Processes and Modeling. *Front Earth Sci.* **2021**, *8*, 576838. [CrossRef]
5. Walvoord, M.A.; Kurylyk, B.L. Hydrologic Impacts of Thawing Permafrost-A Review. *Vadose Zone J.* **2016**, *15*, vzj2016.01.0010. [CrossRef]
6. Shiklomanov, N.I.; Nelson, F.E. Active-layer mapping at regional scales: A 13-year spatial time series for the Kuparuk region, north-central Alaska. *Permafr. Periglac. Process* **2002**, *13*, 219–230. [CrossRef]
7. Zhang, Y.; Carey, S.K.; Quinton, W.L. Evaluation of the algorithms and parameterizations for ground thawing and freezing simulation in permafrost regions. *J. Geophys. Res. Atmos.* **2008**, *113*, 1–17. [CrossRef]
8. Kersten, M.S. Frost penetration: Relationship to air temperature and other factors. *Highw. Res. Board Bull.* **1959**, *225*, 45–80.
9. Jumikis, A.R. *The Frost Penetration Problem in Highway Engineering*; Rutgers University Press: New Brunswick, NJ, USA, 1955.
10. Lunardini, V.J. *Heat Transfer in Cold Climates*; Litton Educational Publishing, Inc.: New York, NY, USA, 1981.
11. Woo, M.K.; Arain, M.A.; Mollinga, M.; Yi, S. A two-directional freeze and thaw algorithm for hydrologic and land surface modelling. *Geophys. Res. Lett.* **2004**, *31*, L12501. [CrossRef]
12. Hayashi, M.; Goeller, N.; Quinton, W.L.; Wright, N. A simple heat-conduction method for simulating the frost-table depth in hydrological models. *Hydrol. Process* **2007**, *21*, 2610–2622. [CrossRef]

13. Kurylyk, B.L.; McKenzie, J.M.; MacQuarrie, K.T.B.; Voss, C.I. Analytical solutions for benchmarking cold regions subsurface water flow and energy transport models: One-dimensional soil thaw with conduction and advection. *Adv. Water Resour.* **2014**, *70*, 172–184. [CrossRef]
14. Changwei, X.; Gough, W.A. A simple thaw-freeze algorithm for a multi-layered soil using the stefan equation. *Permafr. Periglac. Process* **2013**, *24*, 252–260. [CrossRef]
15. Semenova, O.M.; Vinogradova, T.A. A universal approach to runoff processes modelling: Coping with hydrological predictions in data-scarce regions. *IAHS-AISH Publ.* **2009**, *333*, 11–19.
16. Kurylyk, B.L.; Macquarrie, K.T.B. A new analytical solution for assessing climate change impacts on subsurface temperature. *Hydrol. Process* **2014**, *28*, 3161–3172. [CrossRef]
17. Kurylyk, B.L.; Hayashi, M. Improved Stefan Equation Correction Factors to Accommodate Sensible Heat Storage during Soil Freezing or Thawing. *Permafr. Periglac. Process* **2016**, *27*, 189–203. [CrossRef]
18. Kurylyk, B.L.; Watanabe, K. The mathematical representation of freezing and thawing processes in variably-saturated, non-deformable soils. *Adv. Water Resour.* **2013**, *60*, 160–177. [CrossRef]
19. Gouttevin, I.; Krinner, G.; Ciais, P.; Polcher, J.; Legout, C. Multi-scale validation of a new soil freezing scheme for a land-surface model with physically-based hydrology. *Cryosphere* **2012**, *6*, 407–430. [CrossRef]
20. Rawlins, M.A.; Nicolsky, D.J.; McDonald, K.C.; Romanovsky, V.E. Simulating soil freeze/thaw dynamics with an improved pan-Arctic water balance model. *J. Adv. Model. Earth Syst.* **2013**, *5*, 659–675. [CrossRef]
21. Zhang, Y.; Cheng, G.; Li, X.; Han, X.; Wang, L.; Li, H.; Chang, X.; Flerchinger, G.N. Coupling of a simultaneous heat and water model with a distributed hydrological model and evaluation of the combined model in a cold region watershed. *Hydrol. Process* **2013**, *27*, 3762–3776. [CrossRef]
22. Lubini Tshumuka, A.; Krimi, A.; Fuamba, M. Modeling Heat Transfer through Permafrost Soil Subjected to Seasonal Freeze-Thaw. *Land* **2022**, *11*, 1770. [CrossRef]
23. Bergström, S. Development and Application of a Conceptual Runoff Model for Scandinavian Catchments. *SMHI* **1976**, *RHO 7*, 134.
24. Seibert, J.; Bergström, S. A retrospective on hydrological catchment modelling based on half a century with the HBV model. *Hydrol. Earth Syst. Sci.* **2022**, *26*, 1371–1388. [CrossRef]
25. Bergström, S. *The HBV Model: Its Structure and Applications*; Swedish Metorological and Hydrological Institute (SMHI): Norrköping, Sweden, 1992.
26. Lebedeva, L.; Semenova, O.; Vinogradova, T. Simulation of active layer dynamics, Upper Kolyma, Russia, using the hydrograph hydrological model. *Permafr. Periglac. Process* **2014**, *25*, 270–280. [CrossRef]
27. Lebedeva, L.; Semenova, O. Coupled modelling of soil thaw/freeze dynamics and runoff generation in permafrost landscapes, Upper Kolyma, Russia. *IAHS-AISH Proc. Rep.* **2013**, *360*, 118–124.
28. Semenova, O.; Vinogradov, Y.; Vinogradova, T.; Lebedeva, L. Simulation of soil profile heat dynamics and their integration into hydrologic modelling in a permafrost zone. *Permafr. Periglac. Process* **2014**, *25*, 257–269. [CrossRef]
29. Sushansky, S.I. History of creation, methods, objects and some results of studies in the Kolyma water balance station (in Russian). In *Factors Affecting the Formation of a General Drainage System of Minor Mountain Rivers in Sub-Arctic Areas*; Glotov, V., Ukhov, N., Eds.; Svkniidvoran: Magadan, Russia, 2002; pp. 18–35.
30. Makarieva, O.; Nesterova, N.; Lebedeva, L.; Sushansky, S. Water balance and hydrology research in a mountainous permafrost watershed in upland streams of the Kolyma River, Russia: A database from the Kolyma Water-Balance Station, 1948–1997. *Earth Syst. Sci. Data* **2018**, *10*, 689–710. [CrossRef]
31. Bergström, S.; Forsman, A. Development of a conceptual deterministic rainfall-runoff model. *Nord. Hydrol.* **1973**, *4*, 147–170. [CrossRef]
32. Jansen, K.F.; Teuling, A.J.; Craig, J.R.; Dal Molin, M.; Knoben, W.J.M.; Parajka, J.; Vis, M.; Melsen, L.A. Mimicry of a Conceptual Hydrological Model (HBV): What's in a Name? *Water Resour. Res.* **2021**, *57*, e2020WR029143. [CrossRef]
33. Hidalgo, I.G.; Paredes-Arquiola, J.; Andreu, J.; Lerma-Elvira, N.; Lopes, J.E.G.; Cioffi, F. Hydropower generation in future climate scenarios. *Energy Sustain. Dev.* **2020**, *59*, 180–188. [CrossRef]
34. Wijayarathne, D.B.; Coulibaly, P. Identification of hydrological models for operational flood forecasting in St. John's, Newfoundland, Canada. *J. Hydrol. Reg. Stud.* **2020**, *27*, 100646. [CrossRef]
35. Bui, M.T.; Lu, J.; Nie, L. A review of hydrological models applied in the permafrost-dominated Arctic region. *Geoscience* **2020**, *10*, 1–27. [CrossRef]
36. Seibert, J.; Vis, M.J.P. Teaching hydrological modeling with a user-friendly catchment-runoff-model software package. *Hydrol. Earth Syst. Sci.* **2012**, *16*, 3315–3325. [CrossRef]
37. Makarieva, O.; Nesterova, N.; Lebedeva, L.; Sushansky, S. Water-balance and hydrology database for a mountainous permafrost watershed in the up-streams of the Kolyma River, Russia—The Kolyma Water-Balance Station 1948–1997. *PANGAEA* **2017**. [CrossRef]
38. Gusev, E.M.; Nasonova, O.N.; Dzhogan, L.Y. The simulation of runoff from small catchments in the permafrost zone by the SWAP model. *Water Resour.* **2006**, *33*, 115–126. [CrossRef]
39. Kuchment, L.; Gelfan, A. Assessing parameters of physically-based models for poorly gauged basins. *IAHS-AISH Publ.* **2009**, *333*, 3–10.

40. Aghakouchak, A.; Nakhjiri, N.; Habib, E. An educational model for ensemble streamflow simulation and uncertainty analysis. *Hydrol. Earth Syst. Sci.* **2013**, *17*, 445–452. [CrossRef]
41. Hinzman, L.D.; Kane, D.L. Snow hydrology of a headwater Arctic basin: 2. Conceptual analysis and computer modeling. *Water Resour. Res.* **1991**, *27*, 1111–1121. [CrossRef]
42. Liu, L.; Zhang, T.; Wahr, J. InSAR measurements of surface deformation over permafrost on the North Slope of Alaska. *J. Geophys. Res. Earth Surf.* **2010**, *115*, F03023. [CrossRef]
43. Chen, J.; Wu, Y.; O'Connor, M.; Cardenas, M.B.; Schaefer, K.; Michaelides, R.; Kling, G. Active layer freeze-thaw and water storage dynamics in permafrost environments inferred from InSAR. *Remote Sens. Environ.* **2020**, *248*, 112007. [CrossRef]
44. Woo, M.; Steer, P. Slope hydrology as influenced by thawing of the active layer, Resolute, N.W.T. *Can. J. Earth Sci.* **1983**, *20*, 978–986. [CrossRef]
45. Nash, J.E.; Sutcliffe, J.V. River flow forecasting through conceptual models part I—A discussion of principles. *J. Hydrol.* **1970**, *10*, 282–290. [CrossRef]
46. ASCE. Criteria for Evaluation of Watershed Models. *J. Irrig. Drain. Eng.* **1993**, *119*, 429–442. [CrossRef]
47. Gupta, H.V.; Sorooshian, S.; Yapo, P.O. Status of Automatic Calibration for Hydrologic Models: Comparison with Multilevel Expert Calibration. *J. Hydrol. Eng.* **1999**, *4*, 135–143. [CrossRef]
48. Singh, J.; Knapp, H.V.; Arnold, J.G.; Demissie, M. Hydrological Modeling of The Iroquois River Watershed Using Hspf And Swat. *J. Am. Water Resour. Assoc.* **2005**, *41*, 343–360. [CrossRef]
49. Zhuravin, S.A. Features of water balance for small mountainous watersheds in East Siberia: Kolyma Water Balance Station case study. In *Northern Research Basins Water Balance*; Series of Proceedings and Reports; Douglas, L.K., Daqing, Y., Eds.; IAHS Publication: Oxfordshire, UK, 2004; pp. 28–40.
50. Armstrong, R.N.; Pomeroy, J.W.; Martz, L.W. Estimating evaporation in a prairie landscape under drought conditions. *Can. Water Resour. J.* **2010**, *35*, 173–186. [CrossRef]
51. Lebedeva, L.S.; Makarieva, O.M.; Vinogradova, T.A. Spatial variability of the water balance elements in mountain catchments in the North-East Russia (case study of the Kolyma Water Balance Station). *Meteorol. Hydrol.* **2017**, *4*, 90–101.
52. Vinogradov, Y.B.; Semenova, O.M.; Vinogradova, T.A. An approach to the scaling problem in hydrological modelling: The deterministic modelling hydrological system. *Hydrol. Process* **2011**, *25*, 1055–1073. [CrossRef]
53. Semenova, O.; Lebedeva, L.; Vinogradov, Y. Simulation of subsurface heat and water dynamics, and runoff generation in mountainous permafrost conditions, in the Upper Kolyma River basin, Russia. *Hydrogeol. J.* **2013**, *21*, 107–119. [CrossRef]
54. Sugimoto, A.; Naito, D.; Yanagisawa, N.; Ichiyanagi, K.; Kurita, N.; Kubota, J.; Kotake, T.; Ohata, T.; Maximov, T.C.; Fedorov, A.N. Characteristics of soil moisture in permafrost observed in East Siberian taiga with stable isotopes of water. *Hydrol. Process* **2003**, *17*, 1073–1092. [CrossRef]
55. Vionnet, V.; Verville, M.; Fortin, V.; Brugman, M.; Abrahamowicz, M.; Lemay, F.; Thériault, J.M.; Lafaysse, M.; Milbrandt, J.A. Snow Level from Post-Processing of Atmospheric Model Improves Snowfall Estimate and Snowpack Prediction in Mountains. *Water Resour. Res.* **2022**, *58*, e2021WR031778. [CrossRef]
56. Kane, D.L.; Yang, D. *Northern Research Basins Water Balance*; International Association of Hydrological Science: Oxfordshire, UK, 2004.
57. Lebedeva, L.; Semenova, O. Use of soil thawfreeze depth data to verify hydrological_Lebedeva. *Bodenkultur* **2013**, *64*, 53–59.